Acta of Turin Polytechnic University in Tashkent, 2021, 11, 7-20
Published Online June 2021 in Acta TTPU (http://www.acta.polito.uz/)

Design and Structural Performance of Composite Wind Turbine Blade using Finite Element Method

Ibrohim Rustamov
Department of Mechanical and Electrical Engineering, Harbin Engineering University, Harbin 150001, China
Department of Mechanical Engineering, Tashkent State Technical University, Tashkent 100095, Uzbekistan
Email: ibrohimru@yahoo.com

Abstract– In this paper, a 9-meter-long composite wind turbine blade is designed on the basis of blade element theory (BET), and finite element analysis (FEA) is performed using commercial ANSYS software. Various design parameters for a blade such as material properties, laminate lay-up, skin thickness, ply orientation, internal spar etc., are determined iteratively to get optimal blade structural design. NREL S-series airfoils with different chord thickness are used along current blade cross-sections. Glass fibers are traditionally being used as a basis material for wind turbine blade manufacturing. This work also addresses the advanced use of carbon fiber in the spar cap region of the blade as an alternative material. Numerical calculations are run to simulate the static and dynamic characteristics, as well as an Eigen value buckling characteristics in order to confirm the blade to be sound and stable under various load conditions. It is observed that there is a substantial weight reduction and structural strength with the use of cost-effective carbon/glass hybrid material.

Key words– wind turbine blade; structural design; composite materials; finite element method

I Introduction

Wind turbine rotor system includes the hub and blades for converting wind energy to low-speed rotational energy, and accounts for approximately 20% cost of modern wind turbine. Due to the increasing weight and cost of the composite wind turbine blades, researchers all over the world have been investigating alternative composite materials and proper blade design. In several research studies, the use of carbon fiber in the load-bearing spar structure of the blade has been identified as showing moderate promises for cost-effective, weight reduction and increased stiffness. For instance, utilizing carbon fiber spars for a large-scale blade could result in a 38% reduction in total blade mass and a 14% decrease in cost relative to the baseline all fiberglass design [1]. In general, the weight and cost of the turbine are the keys to make wind energy competitive with other sources of power. According to a recent study there is no single component that dominates the turbine cost (tower, nacelle, rotor, drivetrain, power system) but reducing the weight of rotor has a great deal of effect throughout of whole system. Most of the modern turbines have a rotor weight between 37% and 77% of the total weight of the system. Therefore, reducing the weight of the blade is a significant item of research. Further economies might be realized if the carbon fibers can be processed into a form that helps both structural performance and manufacturing efficiency. While carbon fibers tend to have exceptional stiffness and tensile strength properties, realizing the full advantages from carbon fibers will require fabric/preform architectures that also result in good compressive strength [2].

There are many numerical studies that address the structural performance of wind turbine blades by introducing carbon fibers as an alternative material. Ong et al. [3] evaluated the benefit of carbon fibers in a wind turbine blade and explored that hybrid blades had excellent structural properties compared to the all-glass blades. The fabrication processes of a large-scale wind turbine blade using mixed carbon and glass fibers in order to reduce the total weight was reported [4]. Minimization of the blade weight was the main purpose in the study of Veers et al. [5], who described the currently dominant glass fiber technology and the potential use of carbon fibers. Kong and Bang [6] investigated structural design of medium scale composite wind turbine blade by determining design loads from various load cases and fatigue life. A full-scale 34m composite wind turbine blade was tested to failure under flap-wise loading in the work of Jensen et al. [7]. He observed the ovalization of the load carrying box girder in the full-scale test and simulated in non-linear finite element calculations. Jureczko et al. [8] used the BEM theory to design and employed ANSYS to estimate the natural frequencies. They had found out the mode shape of the blades by using the Timoshenko twisted and tapered beam element theory. The genetic algorithm was used to minimize blade vibration, maximize output, minimize blade cost and

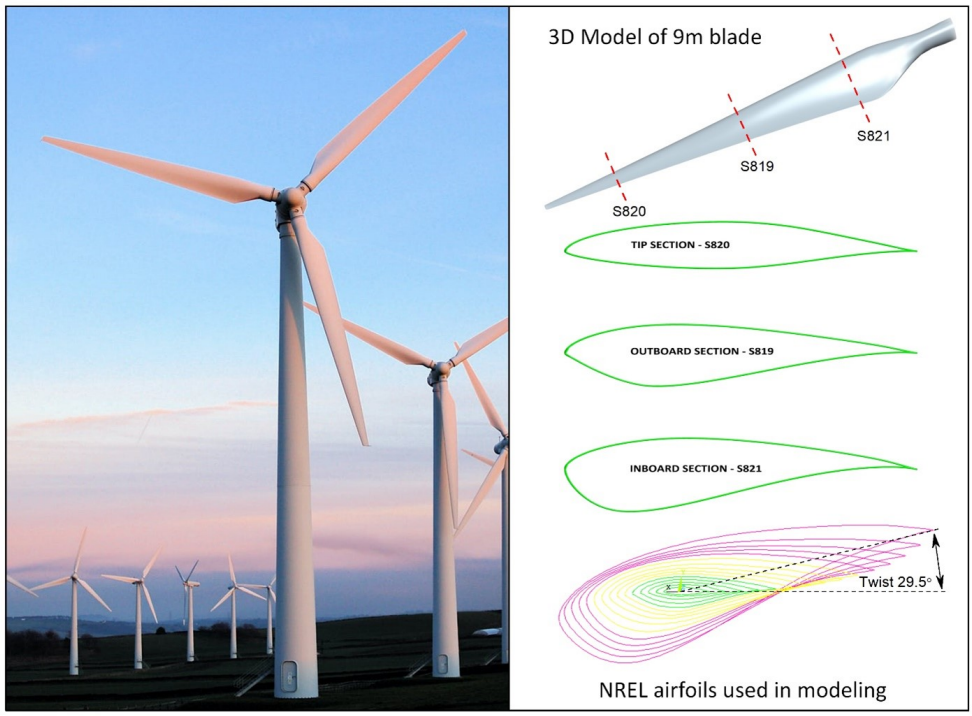

Fig. 1: CX-100 wind turbine (a), and 9-meter-long blade modeling by NREL airfoils (b)

increase stability.

In this paper, a structural design procedure of a composite wind turbine blade was proposed. Utilizing a layered shell element, the geometrical blade model is created by commercial finite element package ANSYS. The main objective of this work involves developing structural finite element model of the wind turbine blade and increasing use of carbon fibers in blade design so as to improve blade performance because of reduced weight and increased strength.

II BLADE STRUCTURAL DESIGN

The external geometry of the representative blade used in this research is based on 9-meter CX-100 (See Figure 1a, originally developed by TPI Composites, Inc and Sandia National Laboratories) medium size 100 kW wind turbine blade with some modifications on the use of materials and stacking sequence of laminates [4]. The S821 root airfoil was used between 20.8% and 40% radius, the S819 primary airfoil was positioned at 70% radius, and the S820 tip airfoil was specified at 95% of the tip radius. Design aspects such as Reynolds number, lift/drag coefficients and tip-speed ratios are listed in Table 1. The skin thickness was reduced along the blade length. The shell also twisted about 29.5 degree owing to the aerodynamic reasons and also has a tapered shape from root to tip. 3D CAD model of the blade has been developed in Pro/E software with the help of text files of airfoil coordinates as shown in Figure 1b.

Final CAD model is then saved as an IGES file to be imported into ANSYS in order to create FE model. Then, the blade is divided into 12 sections and spar cap regions have been defined by using Area by Area inside the Booleans option as shown in Figure 2a. The blade construction is assumed to be a stressed shell, which was composed of four primary components: a low pressure (LP) skin on the downwind side, a high pressure (HP) skin on the upwind side, and a single shear web which is positioned at 35% chord from leading edge bonded between the spar caps inside those skins as depicted in Figure 2b. It runs from root to the tip of the blade and carries shear loads which are directed in transverse. The shear web and outer skin is composed of triaxial and uniaxial fabric separated by a balsa core as filler in sandwich-type layups to provide buckling stability.

III MATERIAL SELECTION

The E-glass/epoxy composite material was selected for the blade skin because of low cost, appropriate fatigue lifetime, desirable specific strength/stiffness, and ease of manufacture. The baseline design uses C520 E-glass unidirectional fibers

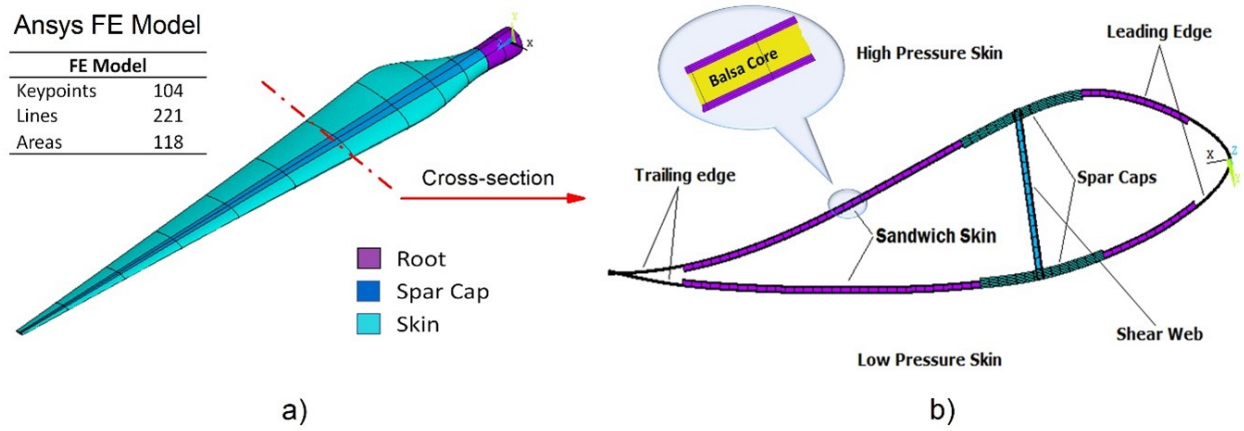

Fig. 2: 3D blade model in ANSYS (a), and structural architecture of the blade (b)

Airfoil	r/R	Reynolds No (x10^6)	Tip-speed ratio	Lift coef. C_{Lmax}	Drag coef. C_{Dmin}
S821	0.40	0.8	0.240	1.4	0.014
S819	0.70	1.0	0.210	1.2	0.008
S820	0.95	1.3	0.160	1.1	0.007

TABLE 1: AIRFOIL DESIGN SPECIFICATIONS ACCORDING TO BET [9]

Properties	Layup Materials				
	C520 (0^0 glass)	C260 ($\pm45^0$ glass)	DBM 1208/1708	Carbon/ glass	Balsa core
E_x (GPa)	37.3	31.7	9.58	84.1	0.12
E_y (GPa)	7.6	7.59	9.58	8.76	0.12
E_z (GPa)	7.6	7.59	6.55	8.76	3.7
ν_{xy}	0.31	0.31	0.39	0.21	0.3
ν_{yz}	0.25	0.31	0.35	0.21	0.01
ν_{xz}	0.25	0.31	0.32	0.21	0.02
G_{xy} (GPa)	6.89	3.52	6.89	4.38	0.02
G_{yz} (GPa)	1.74	3.1	3.72	2.3	0.15
G_{xz} (GPa)	1.74	3.1	3.72	2.3	0.22
υ_f fiber vol	0.52	0.4	0.5	0.52	N/A
ρ (g/cm^3)	1.874	1.75	1.814	1.56	0.23
Thick. (mm)	1.2	0.6	0.56/0.89	0.96	6.35

TABLE 2: MECHANICAL PROPERTIES OF MATERIALS USED FOR BLADE ANALYSIS

in combination with C260 for the lower stiffness glass fiber used in the ±45º and random mat layer for the skin. Spar caps make a use of 80% unidirectional fiber in combination with 20% of DBM (Double Bias Mat) which is fabricated by ±45 degree and stabilized by a continuous strand mat. Balsa core material is used in the trailing edge and the spar shear web as a sandwich material. The resulting assembly provides a structural element with very high bending stiffness, strength and buckling resistance as well as very low weight. As far as the composites are orthotropic materials, they have at least two orthogonal planes of symmetry where the material properties are independent of direction within each plane. The orthotropic materials require nine independent variables in their constitutive matrices. By convention, those elastic con-

No.	Material Description	Plasement Description	Layer Thickness (mm)
1	DBM1708	Outer Skin	0.89
2	Balsa	Fwd Panel	6.35
3	C560 0^0/C260 $\pm45^0$	Spar Cap (Case 1)	1.2
4	Balsa	Aft Panel	6.35
5	DBM1208	Inner Skin	0.56
6	DBM1708	Web Flange	0.89
7	Balsa	Web Core	6.35
8	DBM1708	Web Skin	0.89
9	Carbon 0^0/Glass $\pm45^0$	Spar Cap (Case 2)	0.96

TABLE 3: INTERNAL BLADE STRUCTURAL DESIGN DETAILS

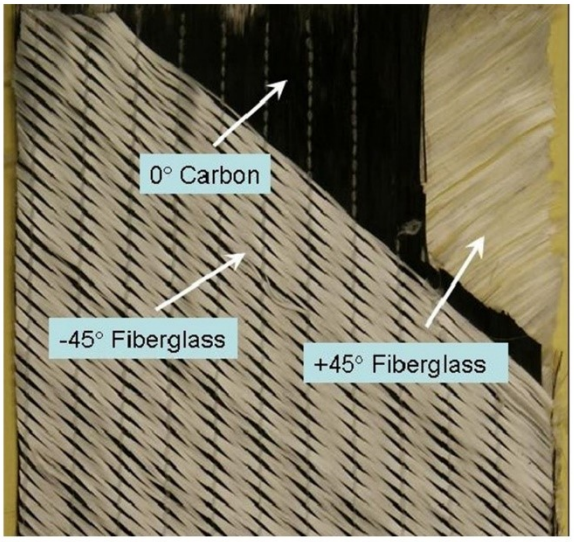

Fig. 3: Triaxial carbon-fiberglass fabric [10]

stants are: Young's modules E_x, E_y, E_z , Poisson's ratios ν_{xy}, ν_{yz}, ν_{xz} and the shear modules G_{xy}, G_{yz}, G_{xz} as listed in Table 2 for each selected material [4, 11].

Relative to fiberglass, the increased stiffness and strength of carbon fiber may improve the structural efficiency and deflection characteristics of slender blade design [10]. A more efficient use of carbon in a carbon/fiberglass hybrid blade is a bulk replacement of the load-carrying unidirectional fibers in the spar material. Unidirectional carbon spar material is well suited to provide the primary flap wise bending strength of the blade and can be efficiently combined with off-axis fiberglass materials (biaxial fabrics) that provide torsional rigidity and retard crack propagation. Concepts of using this hybrid fabric can also be found in references [3, 4, 10, 12]. In order to achieve a high degree of structural coupling in blade laminate, fiberglass spar cap is replaced with triaxial carbon-fiberglass fabric. Therefore, the opportunity for the current blade design to reduce total blade mass is dependent on the extent to which the baseline fiberglass spar caps contribute to the overall blade weight. Figure 3 shows the most favorable fabric carbon-fiberglass triaxial, a multi-layer, multi-axial warp-knit manufactured by SAERTEX [10]. The fiber orientation for this fabric is -45^0 glass/0^0 carbon/+45^0 glass. The net fiber content is 75% carbon and 25% fiberglass by volume. Thus, in this numerical study, we consider the material combination with all-glass (Case 1) and hybrid carbon/glass (Case 2) spar cap material placement to comprehend the effects of carbon fiber in the composite blade structure and its working performance. Table 3 lists the materials distribution and placement for internal structural design of blade station.

IV FINITE ELEMENT METHOD

Analysis can be implemented using ANSYS Parametric Design Language shortly called APDL and/or by the Graphical User Interface (GUI). Both methods are used to increase modeling efficiency. The following section outlines the process used to develop the blade geometry and run a linear static, modal and buckling analysis.

1 Model generation

Whole blade is meshed appropriately with mapped quadrilaterals using Mesh Tool in GUI. The thing to do before meshing is to select proper element types, connect all lines and overlap the areas in order to generate adequate mesh. Because of tapered shape of the blade, thicknesses in the skins will be reduced from root toward the tip. Therefore, a number of Real Constant Sets and layup stacking sequences have been defined with different materials, ply orientation and thicknesses. Then, those different sets can be applied to the elements by using both Meshing Attributes and/or Element Attributes in GUI. The structure of the blade was modeled with the shell elements which is capable of representing layer characteristics throughout the shell thickness. SHELL99, which is used for up to 250 layered applications of a structural model, has six degree of freedom at each node:

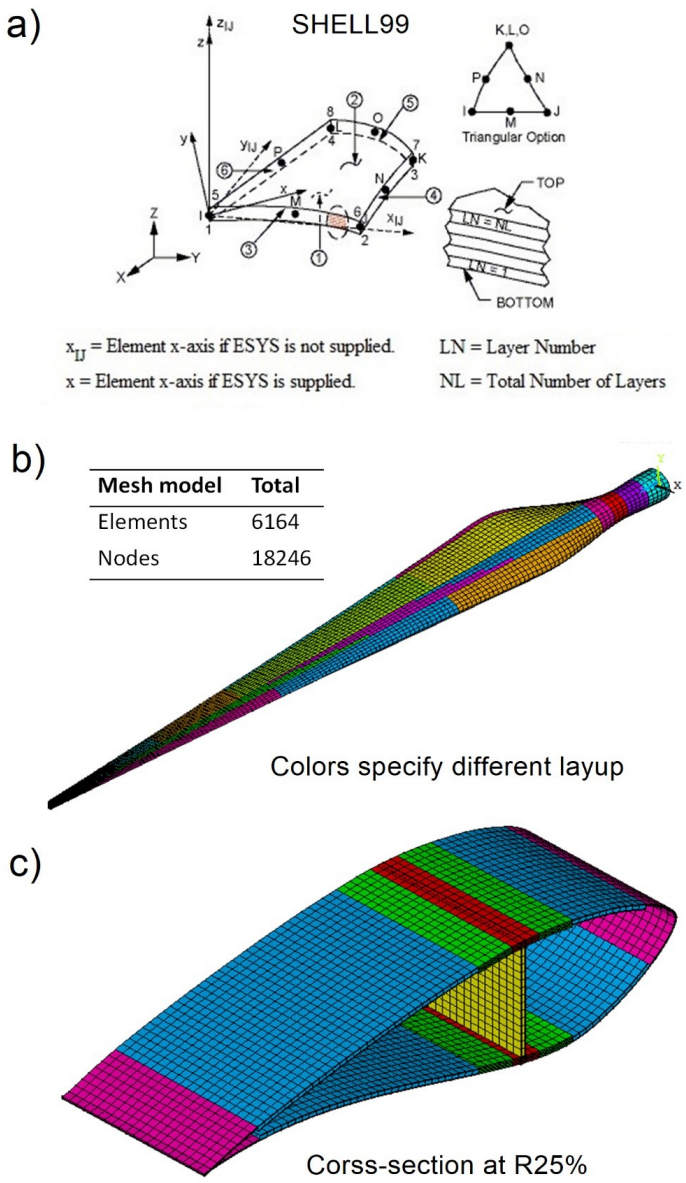

Fig. 4: SHELL99 geometry (a), FE mesh model (b), and cross-section at R25% blade station (c)

translations in the nodal x, y, and z directions and rotations about the nodal x, y, and z axes (See Figure 4a). The final mesh model of the blade is illustrated in Figure 4b with total 6164 elements and 18246 nodes. Colors are used to indicate the different layup stacking and ply thickness along the blade skin and the inner structure as shown in Figure 4c.

2 *Lay-up stacking sequence*

Generally, blade experiences tension/compression stress, bending stress and distorting stress produced by aerodynamic, centrifugal and gravitational loads in its operating process. The blade can be regarded approximately as one-way bearing component. Because the maximum stress generates on blade root, and stress gradually reduces along blade length, the maximum layup thickness should locate in the blade root. Based on composite laminate theory, design structures of different laminates can be determined primarily according to loading characteristic and stress relationship of composite blade. The skin thickness and stacking sequence variations over the blade length are given in Table 4.

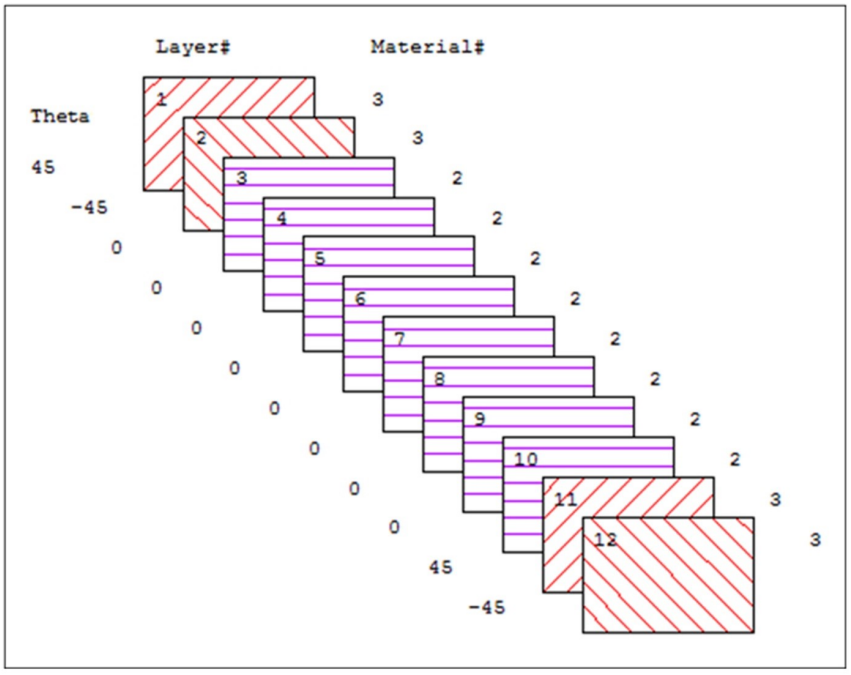

Fig. 5: Stacking sequence for carbon/glass spar cap at R20% station

Components	Station (m)	Layup Schedule	Ply Thickness (mm)
Root	0-0.3	$[\pm45/0_8/\pm45/0_8/\pm45]s$	24.5
	0.3-0.6	$[\pm45/0_6/\pm45/0_6/\pm45]s$	22.1
	0.6-1	$[\pm45/0_4/\pm45/0_4/\pm45]s$	19.7
Spar Cap	1-2.2	$[\pm45/0_8/\pm45]s$	14.9
	2.2-4	$[\pm45/0_6/\pm45]s$	12.5
	4-7	$[\pm45/0_4/\pm45]s$	10.5
	7-9	$[\pm45/0_2/\pm45]s$	8.1
Leading Edge	1-2.2	[±45/0/±45/0/±45]s	4.2
	2.2-6	[±45/0/balsa/0/±45]	9.81
	6-9	[±45/0/±45]S	2.9
Trailing Edge	1-3	[±45/0/balsa/0/±45]	9.25
	3-7.3	[±45/balsa/±45]	8.13
	7.3-9	[±45/0]s	1.78
Shear Web	6-7.2	[±45/±45/balsa/±45/±45]	9.5

TABLE 4: LAYUP SCHEDULE FOR BLADE ANALYSIS

ANSYS supplies the commands for creating, viewing, and listing cross sections, and for managing cross-section libraries. This process can be defined layered sections via GUI (Sections-Shell-Layup-Add/edit). For each layer, the followings are specified in the section definition via the section commands or the section tool accessed with the SECNUM attributes:

1. Material properties;
2. Layer orientation angle commands;
3. Layer thickness.

Figure 5 shows the spar cap layer stacking sequences arranged in ANSYS for carbon/glass substitution on the low-pressure side of the blade. The angle plies provide the skin with torsional stiffness and absorb transverse stresses. And by using unidirectional layers, the high- and low-pressure skins serve for flap-wise stiffness while the leading and trail-

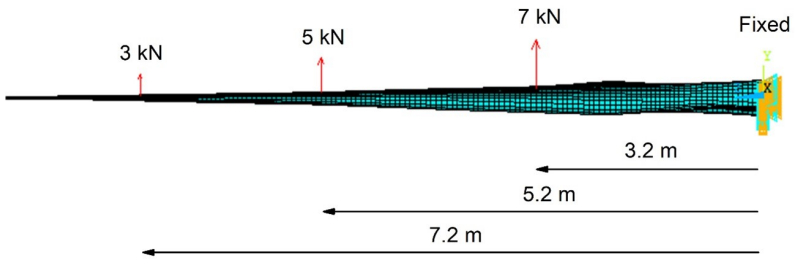

Fig. 6: Blade loading and boundary conditions

ing edges provide the edgewise stiffness.

3 *Loads and boundary conditions*

For this study three load conditions were considered as shown in Figure 6: unit loads of 7 kN, 5 kN and 3 kN were applied perpendicular to the blade surface (y direction) at 3.2 m, 5.2 m and 7. 2 m locations, respectively. The blade was treated as a cantilever beam with the entire model degrees of freedom constrained at the root section. Except this constraint, no other displacement constraints were applied on the blade model. This loading condition is subjected to a flapwise bending load case to approximate the extreme loading events for the wind class to which blade designed [13].

Another important factor in the analysis of a dynamically loaded structure is the study of the free vibration frequencies and corresponding mode shapes, as excitations at or near these frequencies can generate large structural displacements and, as a consequence, large stresses and strains. These natural frequencies are dependent on the fundamental characteristics of the structure, such as geometry, density, and stiffness. Because these same characteristics can be included in an FE model of a structural component, the FE model can be used to determine the natural modes of vibration and corresponding frequencies.

The solution of the equation of motion for natural frequencies and normal modes requires a special reduced form from the equation of motion. If there is no damping and no applied load, the equation of motion in matrix form reduces to:

$$[M]\,[\ddot{u}] + [K]\,[u] = 0 \tag{1}$$

where $[K]$ is the stiffness matrix, that may include centrifugal stiffening effects, $[M]$ is the mass matrix, $\{\ddot{u}\}$ is the nodal acceleration vector, and $\{u\}$ is the nodal displacement vector.

Once the geometry, density, and elastic material models have been defined for the FE model, the dynamic character of the model can be expressed without damping in matrix form as:

$$[K]\,\{u\} - \omega^2\,[M]\,\{u\} = 0 \tag{2}$$

where ω is the circular natural frequency and $\{u\}$ is the Eigen vector that expresses the corresponding mode shape.

The ANSYS program simply uses iterative techniques to determine a set of frequencies and corresponding mode shapes that satisfy the FE matrix equation.

Composites are easy to fail catastrophically, therefore, careful measures must be employed to prevent such an event. A buckling analysis determines the critical load, which leads to structural instability and causes the buckled mode shape. Since it was believed that shell blade design would fail from being overstressed prior to buckling, the faster linear (Eigenvalue) buckling analysis was used. The linear buckling problem of structure is formulated as an eigenvalue problem:

$$([K] + \lambda_i\,[S])\{\psi\}_i = \{0\} \tag{3}$$

where, $[K]$ is stiffness matrix, $[S]$ is stress stiffness matrix, λ_i - ith eigenvalue (used to multiply the loads which generated $[S]$), and ψ_i - ith eigenvector of displacements.

The Block Lanczos eigensolver was used because it is claimed that the solver performs well for models meshed with shell and solid elements. The method used by the modal analysis employs an automated shift strategy, combined with Sturm sequence checks, to extract the number of eigenvalues requested. It has also built-in algorithm for checking convergence, by requesting the eigenvalues to satisfy the convergence ratio:

$$e_i = \left| \frac{(\lambda_i)_n - (\lambda_i)_{n-1}}{B} \right| < T \tag{4}$$

where, $(\lambda_i)_n$ - value of ith eigenvalue in iteration n, $(\lambda_i)_{n-1}$ - value of ith eigenvalue in iteration $n-1$, $B-1$ or $(\lambda_i)_n$, which is greater, T - tolerance value, set to 1E-005.

The eigenvalue buckling analysis must be preceded by a static structural analysis first, with pre-stress effects (PSTRESS) activated. For this analysis, the mass stiffness is replaced with the stress matrix. The analysis is set up using

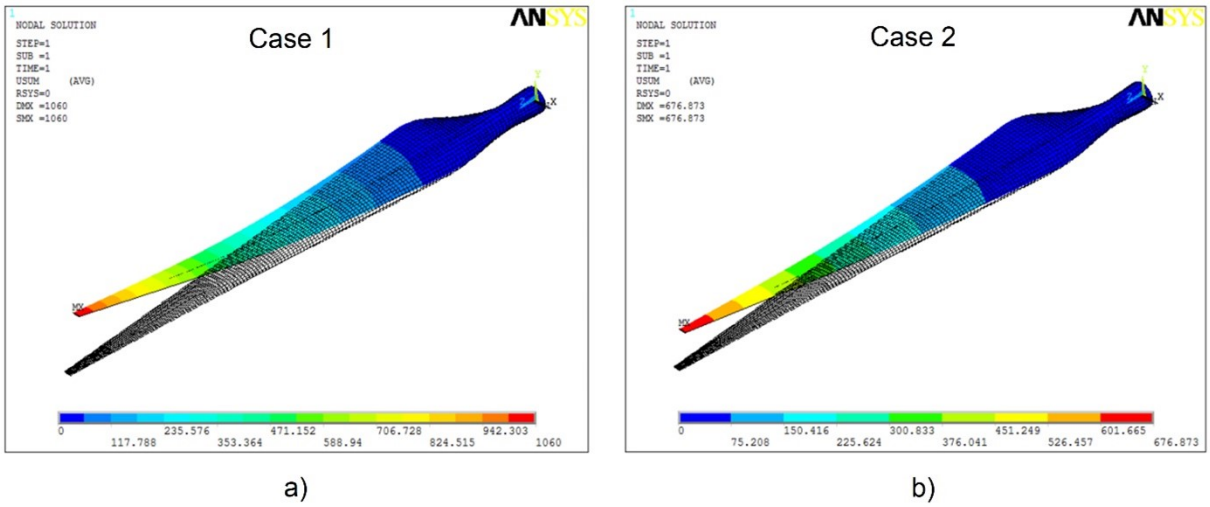

Fig. 7: Blade tip deflections for all-glass blade (a), and carbon/glass hybrid blade (b)

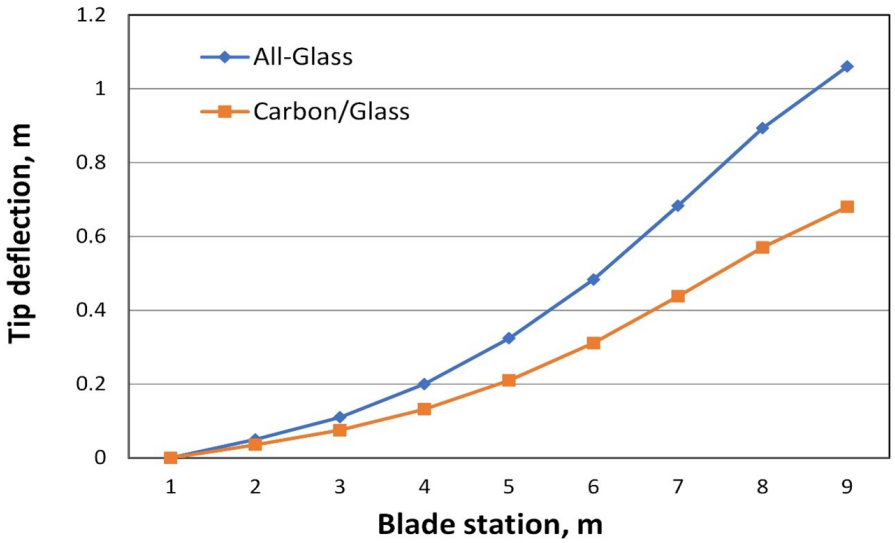

Fig. 8: Comparison of blade deflections for both cases

ANTYPE, BUCKLE in the solution processor (/SOLU). The eigenvalue solution is obtained using the BUCOPT, LANB, 1 command, and the first mode can be expanded using MXPAND, 1. The results are activated and plotted using SET, FIRST and PLDISP, 1. The critical or buckling load factor will be listed as FREQ, since the eigenvalue solution is mostly used for vibration analyses in order to determine natural frequencies.

V RESULTS AND DISCUSSION

1 Blade deflection and stiffness

Generally, there are two issues that are related to the flexural rigidity in the design of a blade. The most important concern is connected with the dynamic behavior of the blade under periodically varying load conditions, like gusting winds. The second concern is blade-tower clearance. If the blade is not sufficiently stiff in the flap-wise direction, the probability of a tower striking and destroying itself under gusty wind conditions increases extensively.

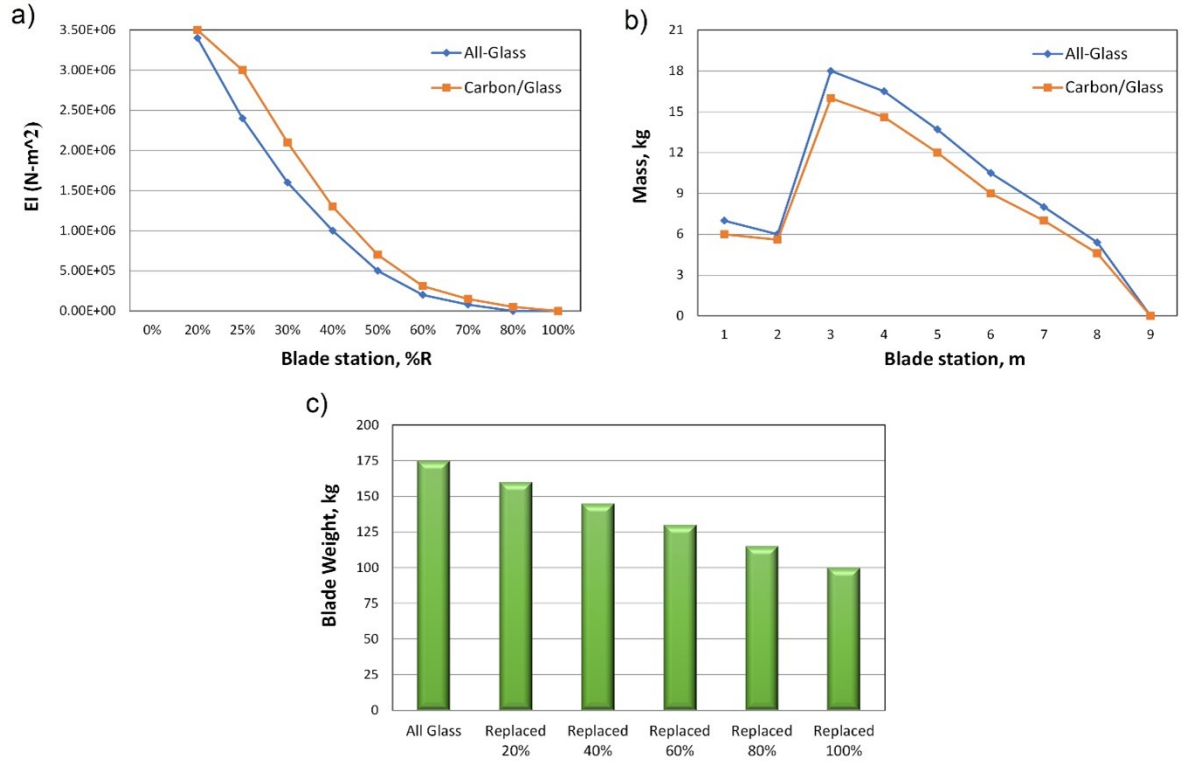

Fig. 9: CComparison of flap-wise bending stiffness (a), estimated mass distribution (b), and total blade weight reduction with carbon fiber use (c

Items	Case1: All-Glass	Case 2: Carbon/glass	$\Delta(\%)$
Total Blade Mass	144.5 kg	128.7 kg	11
Center of Gravity	2.2 m	2.4 m	8,3
Tip Deflection	1.06 m	0.68 m	35.8

TABLE 5: BLADE MASS AND DEFLECTION RESULTS

Blade deflection results are shown in Figure 7 and Figure 8 for both all-glass and hybrid carbon/fiber material layup cases. The largest deflection occurs at the tip and in the direction of lift forces. From the deformed results the vertical deflection was recorded and both the bending angle and bending rate per unit length were calculated. The leading and trailing edge nodes were selected for the angle calculations. As can be seen from the results, maximum deflection for Case 1 is 1.06 m, and Case 2 experiences to have a deflection of 0.68 m. Because the presence of carbon fiber in the load bearing part of the blade, hybrid blade showed exceptional stiffness compared to all-glass blade structure. In the same time, the probability of a tower striking has been reduced significantly with use of carbon fiber.

The bending stiffness can be defined as the ratio of the bending moment M that is transmitted across a given cross-section to the corresponding rate of cross-sectional rotation (θ) per unit length (z). Mathematically, the flexural rigidity can be expressed as:

$$EI = \frac{M}{d\theta/dz} \tag{5}$$

where, E and I modulus of elasticity, moment of inertia, respectively. Figure 9a compares the stiffness distributions of all-glass and hybrid blades. As seen in the figure, the replacement with the carbon spar cap has increased the flap-wise bending stiffness between 20% and 30% over the greater part of the span. It should be noted that the data in Figure 9a have neglected the stiffness increase for the hybrid blade inboard of 25% span. Because of the extent to which the inboard section stiffness will be dominated by the fiberglass root buildup, the presence of the carbon spar in these

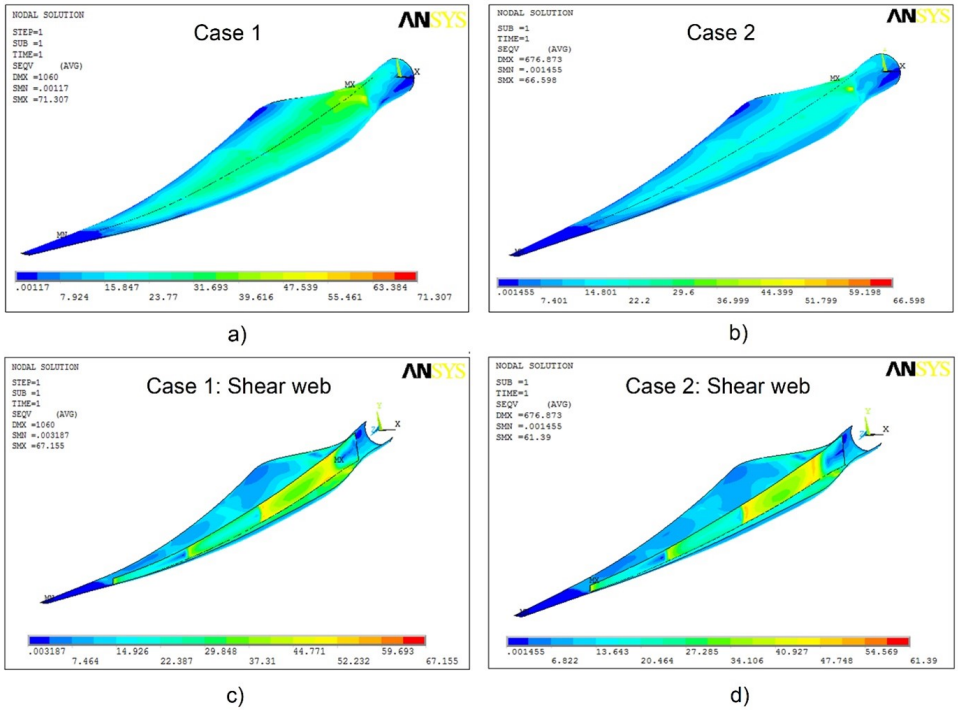

Fig. 10: Von Mises stress for all-glass blade (a, c), and carbon/glass hybrid blade (b, d)

Mode Shapes	Frequency (Hz)	
	Case 1: All-Glass	Case 2: Carbon/Glass
1^{st} Flap-wise	4.7	5.82
1^{st} Edge-wise	6.18	6.93
2^{nd} Flap-wise	11.78	14.41
2^{nd} Edge-wise	18.03	20.12

TABLE 6: COMPARISON OF MODAL ANALYSIS RESULTS

sections was neglected in the carbon/glass design modeling, though in the root transition region, hybrid blade would be slightly stiffer than all-glass due to the continuation of the carbon spar material.

Carbon/glass spar cap has the opportunity to reduce total blade mass. Because, all-glass blade design spar cap weight contributes 20% to 40% of the local blade mass. Inboard of station, the spar cap mass contributions would be even smaller as the fiberglass laminate is increased for root-stud bonding. It is shown in Table 5 that 11% total blade mass reduction of all-glass blade is achieved in the Carbon/glass spar cap design. Figure 9b illustrates resulting mass distributions over both blades in the same time. In Figure 9c, the probability of the blade weight reduction has been plotted by using more carbon fiber replacement in the blade layup construction.

For the blade model, the bending stresses induced by the modeled load distributions are illustrated in Figures 10 for both cases. Blade with all-glass design experiences maximum 71.3 MPa of Von Mises stress, as hybrid blade has maximum 66.5 MPa, demonstrating more strength under extreme conditions. The highest stresses for two blades occur at the root section, while decreasing along the length, approaching zero at the tip section. This is because of decreasing bending moment along the length and constant of inertia moment. However, the current blade designs have a nonlinear decreasing area moment of inertia due to chord length changes and ply drop. As a result of this, the sudden increase in bending stress will take place at 1.2 m of the blade station, where the ply thickness reduces from 12.5 to 6.8 mm, causing a sudden decrease in the area moment of inertia. Except of this region, the stresses decrease along the blade length, remaining modestly unsymmetrical due to the camber of the foil.

The shear web support is incorporated for the shear rigidity and to help in the anchoring to the hub. The majority of the stresses are absorbed into the skin, since the web takes some of the shear loads. From the Figures 10c and d, it is obvious that the shear web experiences the largest bending tensile stress at the root and compressive stress at the first ply drop region near the tip on the LP side. The out of plane shear stress is distributed equally along the web and skin.

When the blade is under load it bends in the direction of the lift forces causing the LP side to be in compression while

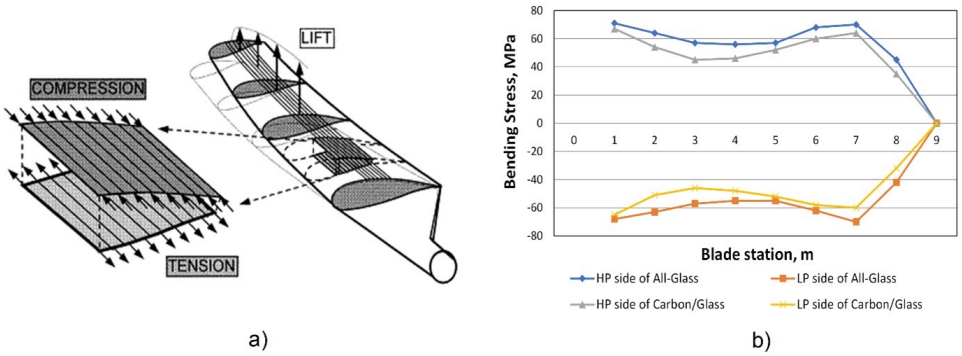

Fig. 11: Illustration of compression and tension on the blade by loading (a), and comparison of stress distributions along the blade (b)

the HP side is in tension as shown in Figure 11a. This trend for Case 1 and Case 2 is illustrated below and can be observed from the results in Figure 11b. Once again, the presence of carbon fiber in the spar cap region leads to better structural characteristics against to the all-glass composition by experiencing lower stress along the blade.

2 Modal shapes and linear buckling

The natural frequencies obtained from the modal analyses are presented for both cases with all-glass and carbon/glass spar cap in Table 6, and Figure 12 provides the mode shapes of all-glass blade. According to the obtained results, hybrid blade with carbon/glass spar cap is slightly stiffer than all-glass blade with generally higher natural frequencies. In a relative sense, no mode varies by more than 1.1% in frequency relative to the mean parameter value. Sometimes, the only desired modes are the lowest frequencies because they can be the most prominent modes at which the object will vibrate, dominating all the higher frequency modes. The pre-stress option is used in ANSYS to specify pre-stress effects which results a constant rotational velocity of 55 rpm. In both cases, the blade was assumed to be rigidly attached to the hub of the turbine at the root section.

The results can be validated using a cantilevered beam model. Because the blades were firmly fastened at the root section and were otherwise free to deform under load, the blade vibrations could be modeled as a cantilevered beam. The first natural frequency (f_1) can be modeled for a prismatic beam by [11]:

$$f_1 = \frac{1.875^2}{2\pi l^2}\sqrt{\frac{EI}{m}} \tag{6}$$

where: l is the length of the beam. Using mean values for the flexural rigidity and mass per unit length, this beam model indicates for the all-glass blade case. And the first natural frequency of the blade is 4.1 Hz, indicating that the finite element method estimation of 4.7 Hz was reasonable for the non-prismatic blade geometry in the given approximate nature of the beam model.

In order to model the blade load for a stationary wind turbine due to such extreme winds, the dynamic pressure on the HP side of the blade is modeled as:

$$P_{hp} = \frac{1}{2}\rho\, v^2 \tag{7}$$

where ρ the air density and v is the wind velocity. Linear buckling is calculated in the 50-year extreme gust wind speed 60 m/s and 0° dangerous position which cause the maximum stress. This wind loads were considered the most likely cause of blade buckling, thus, the blade model was evaluated for possible buckling modes using that pressure distribution. For a 60 m/s wind, the stagnation pressure becomes 4274 Pa. For the FE model, this load was distributed equally in the spanwise direction and as a bilinear gradient with the maximum at the quarter chord position in the chord-wise direction.

First buckling mode shapes are depicted in Figure 13 for both cases. It is obvious, that the buckling took place at approximately 33% of the blade station. Because early results did not meet buckling requirements, additional reinforcements were designed into critical buckling areas in the aft panel and trailing edge region. Balsa wood in the core panels was thickened and extended to the outboard section, and extra unidirectional material were added to the trailing edge region. In addition, the spar thickness was increased in a few critical areas to prevent buckling. As a result, buckling was reduced significantly in the trailing edge outboard of the ply drop.

Corresponding load factors are compared in Table 7. The buckling load factor is an indicator of the factor of safety against buckling or the ratio of the buckling loads to the currently applied loads. The iterative technique to find a set of buckling results in ANSYS was satisfied by Eq. (3). It is clear from results that hybrid carbon/glass blade is found to

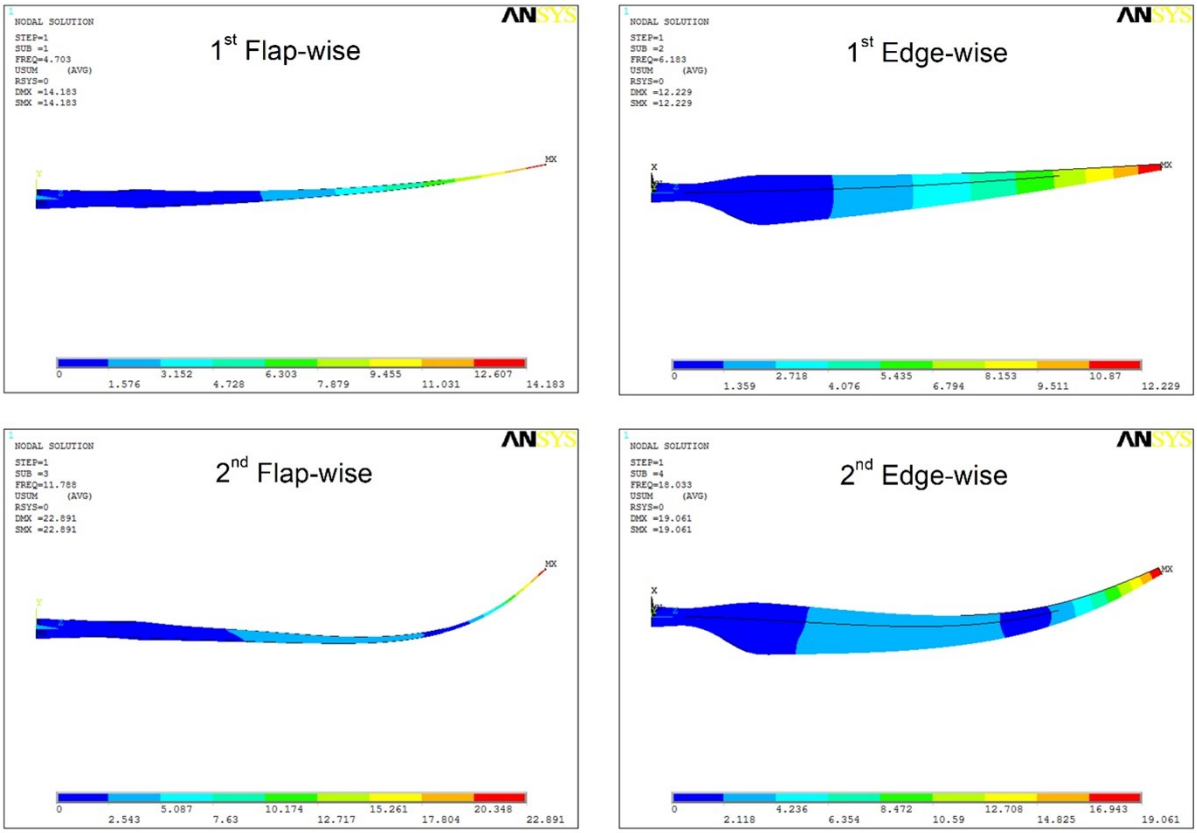

Fig. 12: Modal shapes for all-glass blade

Mode Shapes	Buckling Load Factor (BLF)	
	Case 1: All-Glass	Case 2: Carbon/Glass
1^{st} Mode	1.75	1.49
2^{nd} Mode	1.78	1.50
3^{rd} Mode	1.79	1.60
4^{th} Mode	1.81	1.61

TABLE 7: LOAD FACTORS OF THE BUCKLING MODES UNDER 60M/S WIND SPEED

be more stable and resistant for buckling under the extreme wind conditions.

A baseline of the CX-100 composite blade model is generated and structural analysis has been performed with the help of finite element method. Two different sets of wind turbine blades have been analyzed with iteration techniques until convergence. Carbon fiber is used as an alternative in the load bearing part of the blade and demonstrated excellent stiffness/strength, being safe and sound in contrast to the all-glass blade under extreme weather conditions. This design resulted in total blade weight reduction of approximately 11%, while showing substantial stiffness by 35% increase in blade-tower clearance. The stiffer carbon fibers also resulted in a reduction of the spar cap thickness. These reductions in spar cap thickness also had an impact on the buckling loads. A decrease in the linear buckling load of 15% occurred for the carbon/glass design. All extracted results proved the domination of carbon/glass hybrid blade over the full fiberglass blade in both dynamic and static events.

However, the carbon fiber use in wind turbine blades is more expensive compared to full fiberglass blades, carbon fiber is only applied in cases that design terms are very strict with regard to low weight and high stiffness.

VI CONCLUSION

In this analysis, a fully coupled model of the gas foil bearing is developed by utilizing sophisticated FSI technique for the foil deflection under the hydrodynamic pressure in the film gap through the iterative solving method for the Reynolds equation and structural deformation. Commercial FEA code is employed to accomplish the whole numerical

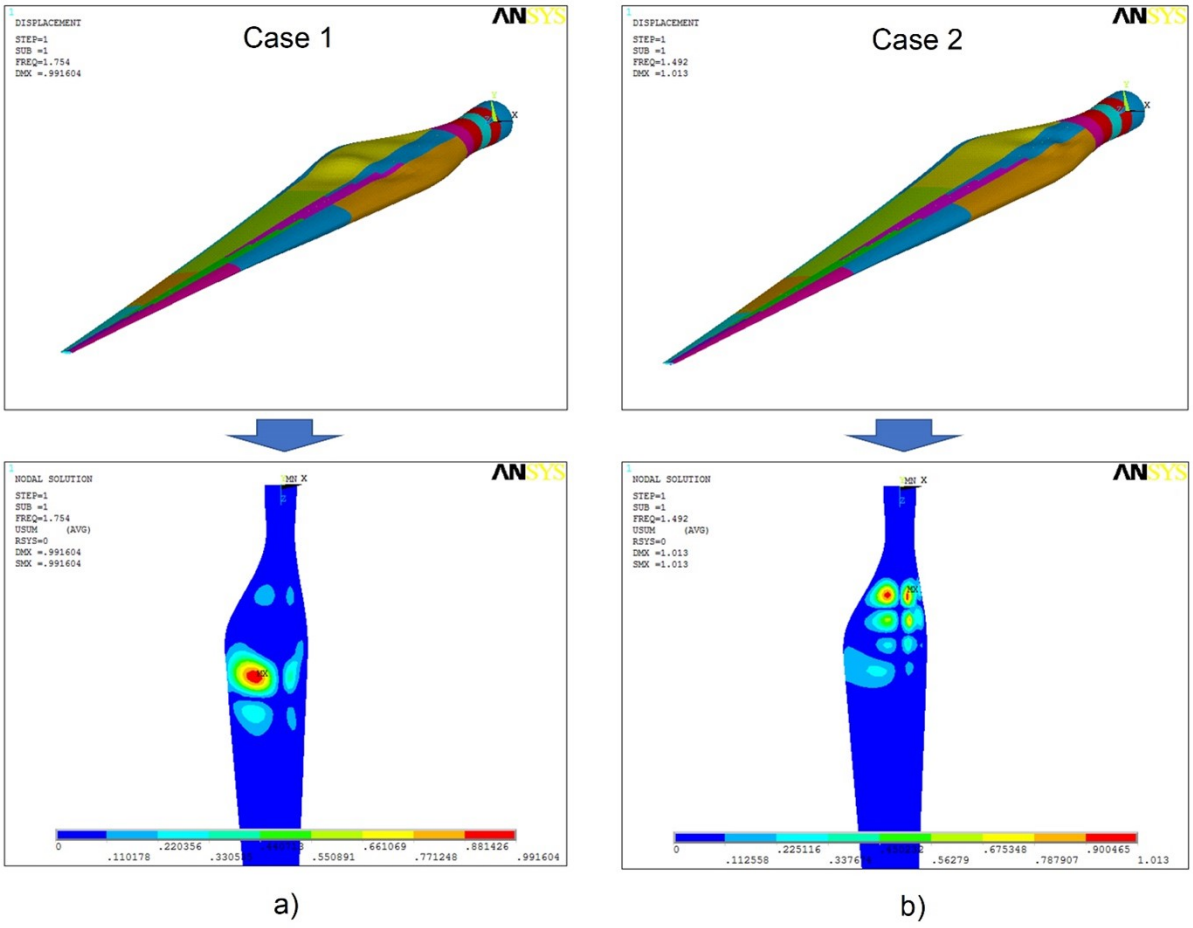

Fig. 13: First Eigen buckling modes for all-glass blade (a), and carbon/glass hybrid blade (b)

procedure with the load transfer capability. The steady-state analysis is conducted for the different parametric cases accounting for the film pressure distributions, film thicknesses, load-carrying capacity and an attitude angle. All obtained numerical results are verified by examining with the existing experimental publications and show good agreement with the test points.

From the results, it can be clearly observed that the film pressure and load-carrying capacity of the bearing is influenced by the eccentricity ratio, angular velocity and L/D ratio of the bearing. Greater load-carrying capacity is due to the higher values of the eccentricity ratio at the higher speeds. The minimum film thickness hmin5 μm is maintained despite of increase in the applied load up to 200 N. As the load and speed increased the film thickness is increased with the relatively small attitude angle. This can be attributed to the foil compliance which can adjust the clearance under the heavy loaded operational conditions. Additionally, the bump foil stiffness enhances the load-carrying capacity i.e. the energy dissipation occurs where the contacting foil surfaces have small amplitudes relative to each other. This type of analysis is concerned with the dynamic properties of the gas foil bearing accounting for Coulomb‘s law which is not considered in this work.

VII Acknowledgement

The author would like to acknowledge the Chinese Government Scholarship (CSC) and Harbin Engineering University (HEU) Scholarship supports for this research work during his Master study in China.

References

[1] James Locke, Ulyses Valencia, and Kosuke Ishikawa. Design studies for twist-coupled wind turbine blades. In *Wind Energy Symposium*, volume 75944, pages 324–

331, 2003.

[2] Dayton A Griffin and Thomas D Ashwill. Alternative composite materials for megawatt-scale wind turbine blades: design considerations and recommended testing. *J. Sol. Energy Eng.*, 125(4):515–521, 2003.

[3] Cheng-Huat Ong and Stephen W Tsai. The use of carbon fibers in wind turbine blade design: a seri-8 blade example. 2000.

[4] Derek Berry and T Ashwill. Design of 9-meter carbon-fiberglass prototype blades: Cx-100 and tx-100. *SAND2007-0201, Sandia National Laboratories, Albuquerque, NM*, 2007.

[5] Paul S Veers, Thomas D Ashwill, Herbert J Sutherland, Daniel L Laird, Donald W Lobitz, Dayton A Griffin, John F Mandell, Walter D Musial, Kevin Jackson, Michael Zuteck, et al. Trends in the design, manufacture and evaluation of wind turbine blades. *Wind Energy: An International Journal for Progress and Applications in Wind Power Conversion Technology*, 6(3):245–259, 2003.

[6] Changduk Kong, J Bang, and Y Sugiyama. Structural investigation of composite wind turbine blade considering various load cases and fatigue life. *Energy*, 30(11-12):2101–2114, 2005.

[7] FM Jensen, BG Falzon, J Ankersen, and H Stang. Structural testing and numerical simulation of a 34 m composite wind turbine blade. *Composite structures*, 76(1-2):52–61, 2006.

[8] MEZYK Jureczko, M Pawlak, and A Mężyk. Optimisation of wind turbine blades. *Journal of materials processing technology*, 167(2-3):463–471, 2005.

[9] JL Tanglers and DM Somers. Nrel airfoil families for small hawt. *Proceedings of AWEA*, pages NREL–TP, 1995.

[10] Dayton A Griffin. Blade system design study. part ii, final project report (gec). Technical report, Sandia National Laboratories, 2009.

[11] Ladean R McKittrick, Douglas S Cairns, John Mandell, David C Combs, Donald A Rabern, and R Daniel Van Luchene. Analysis of a composite blade design for the aoc 15/50 wind turbine using a finite element model. *Sandia national laboratories report*, 2001.

[12] Dayton A Griffin and Michael D Zuteck. Scaling of composite wind turbine blades for rotors of 80 to 120 meter diameter. *J. Sol. Energy Eng.*, 123(4):310–318, 2001.

[13] Joshua Paquette, Daniel Laird, Daniel Griffith, and Laura Rip. Modeling and testing of 9m research blades. In *44th AIAA Aerospace Sciences Meeting and Exhibit*, page 1199, 2006.